Growth and Fabrication of High-Quality Single Nanowire Devices with Radial p-i-n Junctions

Yunyan Zhang, Ana M. Sanchez, Martin Aagesen, Suguo Huo, H. Aruni Fonseka, James A. Gott, Dongyoung Kim, Xuezhe Yu, Xingyou Chen, Jia Xu, Tianyi Li, Haotian Zeng, Giorgos Boras, and Huiyun Liu*

Nanowires (NWs) with radial p-i-n junction have advantages, such as large junction area and small influence from the surface states, which can lead to highly efficient material use and good device quantum efficiency. However, it is difficult to make high-quality core–shell NW devices, especially single NW devices. Here, the key factors during the growth and fabrication process that influence the quality of single core–shell p-i-n NW devices are studied using GaAs(P) NW photovoltaics as an example. By p-doping and annealing, good ohmic contact is achieved on NWs with a diameter as small as 50–60 nm. Single NW photovoltaics are subsequently developed and a record fill factor of 80.5% is shown. These results bring valuable information for making single NW devices, which can further benefit the development of high-density integration circuits.

III–V Nanowires (NWs) have attracted significant attention, due to their novel mechanical, optical, and electronic properties that are not present in the thin film counterparts,[1–5] and diverse types of NW-based devices have been demonstrated across a wide range of applications. For example, NWs are highly attractive as the basis for future photovoltaics. They can provide superior photon harvesting functions compared with thin-film devices due to the 1D structure, subwavelength diameter, and high refractive index. The electromagnetic modes of the horizontal NWs tend to be leaky and the leaky-mode resonances can induce field enhancements inside nanostructures to spectrally tune and enhance fundamental absorption properties.[6,7] For vertically standing NWs, the absorption cross section can be greatly enlarged, which is much bigger than their physical size.[8] When using these NWs to form arrays or randomly positioned forests, it can bring outstanding antireflection and light-trapping properties,[9–11] which can further enhance light absorption.[12–15]

NWs have a large surface-to-volume ratio and hence high-density of surface states. Study from Christesen et al.[16] revealed that the NW devices with radial p-i-n structures are "surprisingly insensitive to surface recombination" compared to the ones with axial structures. The internal quantum efficiencies of radial devices can be as high as 95% even with high surface recombination velocities (SRVs) of 10^5 cm s^{-1}; while axial devices require substantially lower values of 10^3–10^4 cm s^{-1} to produce the same level of performance because their depletion region is exposed to the surface. Apart from quantum efficiency, the open-circuit voltages of their radial devices are nearly twice that of axial devices. When the radial p-i-n structure is used in photovoltaics, it is superior in extracting the generated carriers compared to the thin-film structures. The collection efficiency of generated carriers depends strongly on the minority carrier diffusion length, which decreases with increasing defect density.[17] Most generated carriers will be wasted if they are more than one diffusion length away from the space charge region. For the traditional thin-film device, the collection path of the generated carriers is parallel to the solar photon travelling path.[18,19] Therefore, the requirement for a thick enough absorption material puts high demand on the crystal quality, so that the carriers can pass through without substantial recombination. In the case of the NW, light absorption and carrier extraction are decoupled for the core–shell p–n junction device. It absorbs the light along the whole NW, while the generated carriers can be efficiently separated in the radial direction. The radial distance that carriers need to travel through (hundreds

Dr. Y. Zhang, D. Kim, Dr. X. Yu, J. Xu, H. Zeng, G. Boras, Prof. H. Liu
Department of Electronic and Electrical Engineering
University College London
London WC1E 7JE, UK
E-mail: yunyang.zhang.11@ucl.ac.uk

Prof. A. M. Sanchez, Dr. H. A. Fonseka, J. A. Gott
Department of Physics
University of Warwick
Coventry CV4 7AL, UK

Dr. M. Aagesen
Center for Quantum Devices
Niels Bohr Institute
University of Copenhagen
Universitetsparken 5, 2100 Copenhagen, Denmark

Dr. S. Huo, Dr. T. Li
London Centre for Nanotechnology
University College London
London WC1H 0AH, UK

Prof. X. Chen
State Key Laboratory of Functional Materials for Informatics
Shanghai Institute of Microsystem and Information Technology
Chinese Academy of Sciences
Shanghai 200050, China

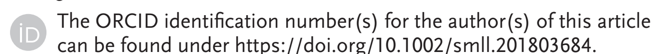
The ORCID identification number(s) for the author(s) of this article can be found under https://doi.org/10.1002/smll.201803684.

© 2018 The Authors. Published by WILEY-VCH Verlag GmbH & Co. KGaA, Weinheim. This is an open access article under the terms of the Creative Commons Attribution License, which permits use, distribution and reproduction in any medium, provided the original work is properly cited.

The copyright line for this article was changed on January 18, 2019 after original online publication.

DOI: 10.1002/smll.201803684

of nanometers) is normally much smaller than, or comparable with, the minority carrier diffusion length (in micrometer range). Therefore, the orthogonally decoupled light absorption and carrier separation paths can lead to low recombination, and hence high efficiency. In addition, the NWs have large surface-to-volume ratio, which offers large junction area, that are hundred times larger compared with axial junctions and can further enhance the charge separation efficiency. All those advantages enable us to use lower-purity and less-expensive materials with low minority carrier diffusion lengths. As a result, the use of NW structure can significantly reduce the device cost.

Divided by size, there are large-area[20–26] and single NW devices. The fabrication of large-area devices frequently faces the difficulty of pinpointing the bottle necks, as there are many factors that can limit the device performances. Studying single NW devices helps large-area devices by identifying the intrinsic limiting factors caused by NW itself and provide valuable information on ways of improvement. Moreover, single NW devices can be used in high-density integrated circuits (ICs). For example, Si-based photonics as a next generation IC technology requires a large number of photon detectors to support the optical interconnections.[27] Integrating single III–V NW photon detector with Si microelectronics, may greatly facilitate the chip-to-chip and system-to-system optical communications.

There has been extensive study of the fabrication of single NW devices, such as solar cells (SCs) and detectors.[28–30] However, most of them are axial p-i-n structures because it is comparatively easy to fabricate contacts.[31,32] There are some reports which focus on radial p-i-n structure, but most of the devices are limited in performance.[33,34] NW doping is the first challenge in device fabrication. High-concentration doping is critical to achieve a good Ohmic contact.[35,36] However, doping of NWs is more complex than that in thin-film growth and it is still unknown whether the doping concentration and quality in NWs can support the formation of good Ohmic contacts.[37] For the widely used self-catalyzed NWs, the vapor–liquid–solid (VLS) growth mode makes it difficult to dope the core NW into n-type. The core NW is thus commonly p-type doped and then covered by i- and n-shells to form p-i-n junction. The p-doping of self-catalyzed core NWs is controlled by the catalytic droplet.[37] The liquid growth environment, high growth temperature, and proximity to thermodynamic equilibrium at the growth front can significantly limit the incorporation of p-dopants and further affect the contact quality.[37] Besides, for ternary materials with the advantage of large composition and hence bandgap tunability, there is however no study on the influence of composition on the doping properties. Shell removal is the second challenge in device fabrication. To make p-type contact the n- and i-shells must be removed and then contact metal deposited onto the exposed p-regions. Due to the small size, it is difficult to perform the shell removal uniformly and precisely there is still no systematic study on the shell removal. The high density of NW surface states is the third challenge in device fabrication. The high-density of surface states can pin the Fermi level at the NW surface to the middle of the bandgap.[38][39] When NWs contact with metal, the pinning can produce a Schottky barrier and seriously hinder the formation of Ohmic contact. It has been reported that unpassivated GaAs NWs will be seriously depleted when the diameter is below 100 nm, making the Ohmic contact formation even more difficult.[40] Therefore, most of the single NW photovoltaics with the core–shell p-i-n structure have low fill factors (commonly <70%).[29] To the best of our knowledge, there is only one report that presents single core–shell p-i-n NW SC with a fill factor over 70%.[41] However, there is still lack of the detailed and systematic study on how to make good Ohmic contact on this core–shell p-i-n type of NWs to form high-quality devices.

The working wavelength of GaAsP can be adjusted ranging from green to infrared, which is one of the most promising photovoltaic materials. Especially, it has been predicted that a two-junction tandem SC, consisting of a 1.7 eV GaAsP NW junction and a 1.1 eV Si junction, has a theoretical efficiency of 33.8%/42.3% at 1 sun/500 suns AM1.5D condition, which can open a way to make high-efficiency low-cost SCs.[42] Therefore, in this article, the key factors that can strongly affect the quality of single core–shell p-i-n NW devices have been investigated in detail with GaAsP NW photovoltaics, such as p-type doping of core and shell, removal of n- and i-shells, and annealing of the contact. This study leads to the fabrication of single NW photovoltaics with a fill factor of 80.5%. So far as we know, this is the highest value in NW photovoltaic field, including devices with the axial junction.

GaAs NWs with different Beryllium (Be) doping levels were first grown using Ga-catalyzed VLS mode on Si (111) substrates by molecular beam epitaxy (MBE).[43] As can be seen from the scanning electron microscope (SEM) image shown in **Figure 1**a, when the GaAs NWs are undoped, they are highly uniform in diameter (50–60 nm) along their entire length (3–4 µm). There is a round Ga droplet at the exact top of each NW, which clearly indicates the VLS growth mode. When they are doped with a nominal doping concentration of 6.4×10^{18} cm^{-3}, the NWs remain uniform in diameter, but the droplets are displaced from the NW center (Figure 1b), indicating that the Be changes the vapor–liquid and liquid–solid interface energies leading to droplet sidewall wetting. Further increase in the nominal doping concentration to 1.28×10^{19} cm^{-3} (Figure 1c), the NW tip is kinked and enlarged with an elongated cross section (right inset of Figure 1c). This is because the high Be concentration inside the droplets causes the imbalance of interface energies and hence the droplet instability. When the surface energies pass the point where the maximum stable contact angle is exceeded, the droplet moves from the top to the sidewall and axial growth ceases.[44] After the droplet slides to the side wall, its solidification leads to the creation of new facets. Those new facets have higher surface energy than the originally bonded (110) facets and provide more favorable nucleation sites for the parasitic vapor-solid (VS) growth.[45] Among all the new facets, the ones facing down can develop much faster. This is because they can form a concave area (yellow arrows in Figure 1b,c) with the help of the NW sidewalls below. This concave area has low surface chemical potential and hence has more advantages to collect source materials.[46] As a result, the parasitic growth starts from the kinked tip and develops downward (Figure 1d). In addition, because the droplet can only move to one side of the NW, the opposite side is still bounded by low-energy {110} facets. Therefore, parasitic growth occurs only on the side to which the

© 2018 The Authors. Published by WILEY-VCH Verlag GmbH & Co. KGaA, Weinheim

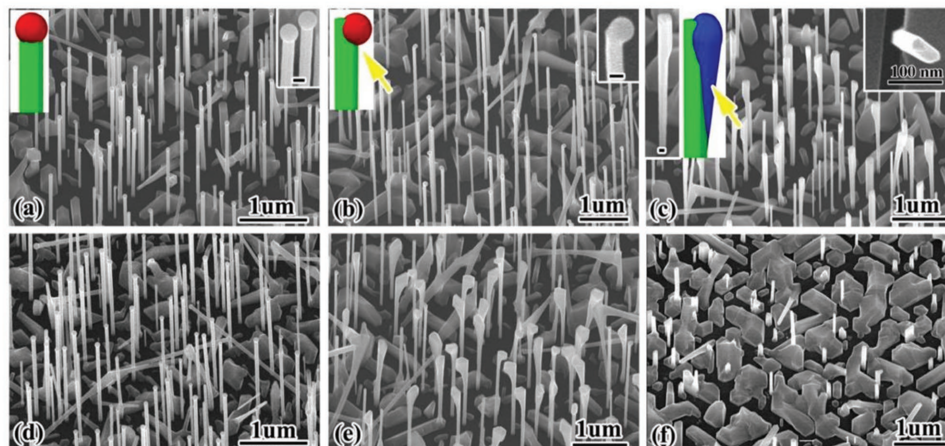

Figure 1. a–c) SEM image of GaAs NWs with a nominal doping concentration of 0, 6.4×10^{18}, and 12.8×10^{18} cm^{-3}, respectively. The insets in (a) and (b) are SEM images and illustrations that show the detailed features of the NW tips. The right inset in (c) is the top view of a NW that shows an elongated cross section. The unnumbered scale bars are 50 nm. d–f) SEM image of $GaAs_{0.8}P_{0.2}$ NWs with a nominal doping concentration of 0, 6.4×10^{18}, and 8.9×10^{18} cm^{-3}, respectively.

droplet moves. This unsymmetrical development leads to an elongated cross section as shown in inset of Figure 1c.

As a comparison, $GaAs_{0.8}P_{0.2}$ NWs with different doping concentration were grown. As can be seen in Figure 1d, the morphology of undoped GaAsP NW is quite similar to that of undoped GaAs NWs shown in Figure 1a. They are also highly uniform in diameter along the NW length and with a round Ga droplet at the exact top of each NW. With the introduction of a nominal doping concentration of 6.4×10^{18} cm^{-3}, the NW tip is kinked and enlarged with an elongated cross section. This is in stark contrast to the NWs shown in Figure 1b despite the same nominal doping concentration, but quite similar to the NWs shown in Figure 1c that with a higher nominal doping concentration. Further increase the nominal doping concentration to 8.9×10^{18} cm^{-3}, the NWs were hardly grown, though the doping flux is much lower than that of Figure 1c sample.

From the comparison, it can be seen that the GaAsP NW are suffering stronger influence from Be doping compared with GaAs NWs. This can be because the bond between Ga and P is stronger than that between Ga and As.[47] With the increase of P in the NW, it is more difficult for Be atom to be incorporated as it needs to overcome higher energy barriers.[48] Therefore, the Be accumulation inside the Ga droplet is faster for NWs grown with higher P content, especially under high doping flux.

To achieve better Ohmic p-contact and to construct p-i-n junction, it is necessary to grow a layer of p-type shell on the p-core. The shell growth uses the vapor–solid growth mode that is the same as thin-film growth. However, self-catalyzed NWs are bounded by {110} facets that have much lower surface energy than {100} thin-film substrates. This makes the shell growth conditions rather different from that of thin-film growth, especially the temperature and III–V flux ratio. This can significantly influence shell doping levels. Besides, the NWs are commonly observed to have high-densities of stacking faults, such as twins or a mixture of zinc blende (ZB) and wurtzite (WZ) crystal structures, which can also affect the doping process.

To study the inter-action between the Be doping and shell growth, core–shell GaAsP NWs with different nominal shell doping concentrations were grown. As can be seen in **Figure 2**a,b, NWs with the undoped and slightly doped (1×10^{17} cm^{-3}) shells have very smooth sidewalls despite the presence of stacking faults which can be seen from the transmission electron microscopy (TEM) image (inset Figure 2b). Further increase in the nominal doping concentration of shell to 6×10^{18} cm^{-3}, the NWs have enlarged lumps along the length of the NW (Figure 2c). Each lump has a twin plane across its widest diameter (inset Figure 2c). The reduction of the shell growth temperature by 40 °C can reduce the lump size, but the NWs still have a rough surface with high density of defects (Figure 2d).

These phenomena can be explained by the surface energy. The stacking faults can create new facets with higher surface energy than {110} facets at the surface, making the nucleation at these sites energetically preferable. When there is no or low-concentration Be doping, the shell growth is still uniform which could be because, at the low growth temperatures employed (500 °C), the Ga mobility is not high enough to cause long-distance re-distribution. When the shell is grown with a high concentration of Be dopants, the mobility of Ga adatoms is significantly improved due to the surfactant effect of Be.[49] Ga with enhanced mobility has a greater ability to move to and nucleate at these locations with stacking faults. This results in these areas growing much faster than the defect-free locations and, therefore, forming the lumps. The mobility of Ga reduces with the shell growth temperature, which can relieve the lump-forming phenomena, however is not effective enough to retrieve the morphology and crystal quality of the highly doped shells.

A study of p-contact was performed using pure GaAs NWs. The use of pure GaAs NWs eliminates the influences of composition difference or fluctuation. AuZn contacts (Zn% = 5%) were made on Be-doped GaAs NWs with a 2-contact configuration (inset **Figure 3**a). They have a diameter of 50–60 nm, which is far below the depletion threshold of 100 nm.[40] As

© 2018 The Authors. Published by WILEY-VCH Verlag GmbH & Co. KGaA, Weinheim

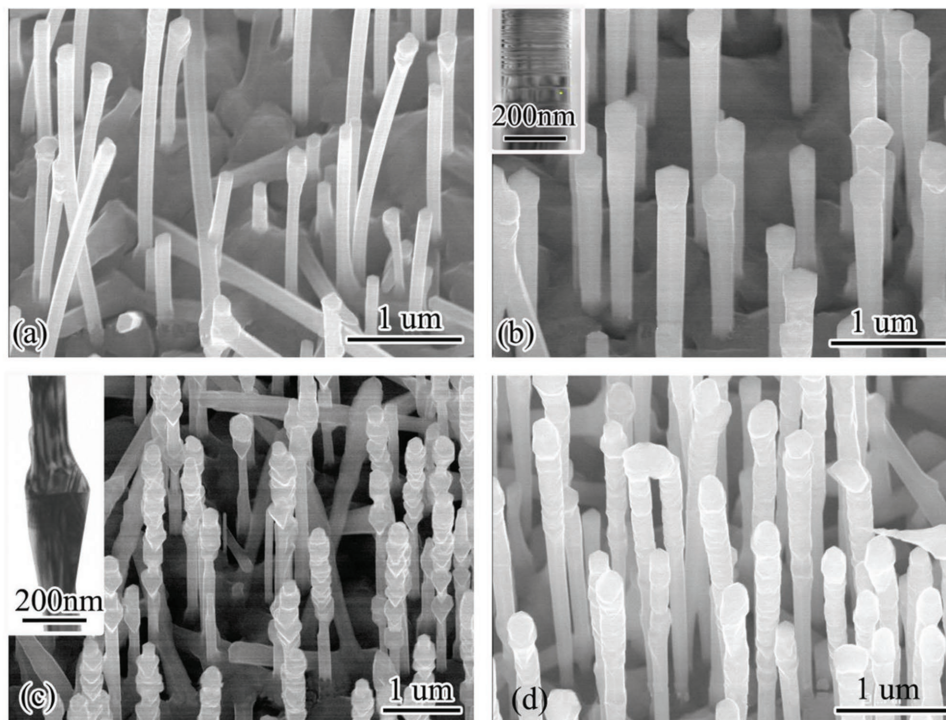

Figure 2. a–c) SEM image of GaAsP NWs with a nominal shell doping concentration of 0, 1×10^{17}, and 6×10^{18} cm^{-3}, respectively. The inset in (b) is a TEM image that shows high-density stacking faults. The inset in (c) is a TEM image that shows a single twin. d) SEM image of core–shell GaAsP NWs grown at similar condition as (c) but the shell growth temperature was 40 °C lower.

shown in Figure 3a, the as-made Be-doped NW devices show Schottky contact with high resistance. During annealing in a N_2 atmosphere, the Schottky barrier height gradually decreased (Figure 3a) and eventually changed to Ohmic at an annealing temperature of 380 °C (Figure 3b). The annealing can also help the formation of Ohmic contact on undoped GaAs NWs. However, the resistance is more than one order of magnitude higher, which suggests that p-doping is necessary to achieve a good Ohmic contact. This result shows that the NW can still realize Ohmic contact with a diameter as small as 50–60 nm. So far as we know, this is the smallest III–V NWs with Ohmic contacts.

GaAs NW photovoltaics with a radial p-i-n junction were grown. As can be seen in **Figure 4**a, these NWs have smooth surface, despite the presence of some sparsely located twins shown in Figure 4b–d. To passivate the surface, an AlGaAs passivation layer and an outer GaAs protection layer were grown. As can be seen in the longitudinal cross section shown in Figure 4e, two darker gray strips are present close to the surface, suggesting an Al-rich shell. This is confirmed by energy-dispersive X-ray spectroscopy (EDX) cross section (inset of Figure 4e) and mapping (Figure 4f–h). The axial cross section is also shown in Figure 4i. The core–shell NW has a hexagonal shape and the AlGaAs shell is continuous and relatively uniform (Figure 4 j–l).

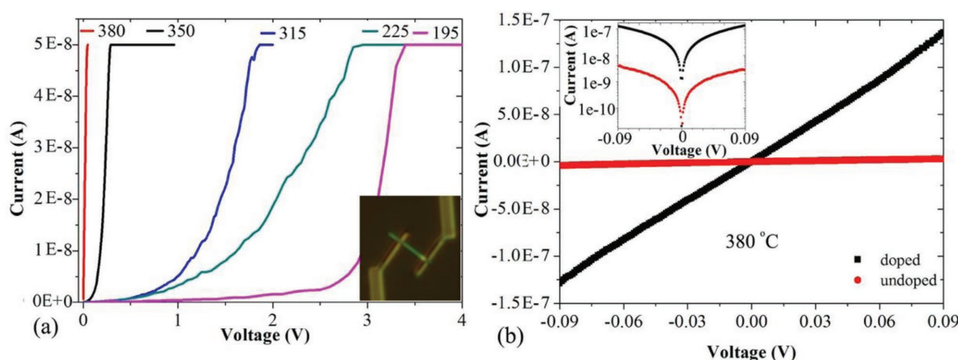

Figure 3. a) *I–V* characteristics of p-doped GaAs NWs (6.4×10^{18} cm^{-3}) measured with a single 2-contact configuration shown in its inset. The contact was annealed with different temperatures marked on top of each curve (380, 350, 315, 225, 195 °C). b) The *I–V* characteristics of undoped and doped GaAs NWs with contacts annealed at 380 °C.

© 2018 The Authors. Published by WILEY-VCH Verlag GmbH & Co. KGaA, Weinheim

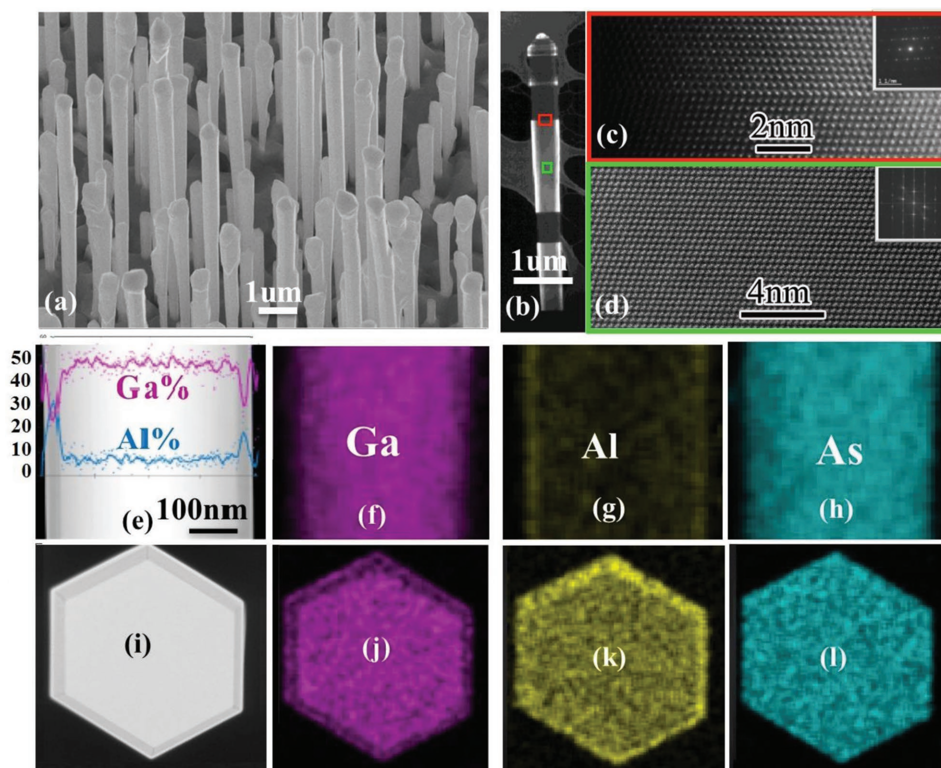

Figure 4. a) SEM image of GaAs NW photovoltaics grown with a radial p-i-n junction. b) Low-resolution TEM image show a NW with occasional twinning. Atomic resolution TEM images show c) a single twin plane and d) stacking-fault-free regions. The insets are two electron diffraction patterns, which show the twins and the stacking-fault-free feature. e) Annular dark field scanning transmission electron microscopy (ADF-STEM) image of the longitudinal cross section. The overlay plot is the EDX profile of Al, Ga, and As. EDX maps of f) Ga, g) Al, and h) As. i) ADF-STEM image of the axial cross section. EDX maps of j) Ga, k) Al, and l) As.

To contact the p-core, the n- and i-shells must be removed. In thin-film device fabrication, this is commonly done by wet etching using H_3PO_4:H_2O_2:H_2O.[50] Therefore, wet etching by H_3PO_4:H_2O_2:H_2O (1:1:60) were performed for 1–2 min on core–shell GaAs NWs with good morphology (**Figure 5**a). As can be seen in Figure 5b,c, after etching, the diameter of NWs is no longer uniform. There are some over-etched parts and the ring-shaped etching indicates the presence of stacking faults in these regions. The stacking faults can be more easily corroded and etching speed is therefore faster around these regions. Interestingly, this suggests that chemical wet etching

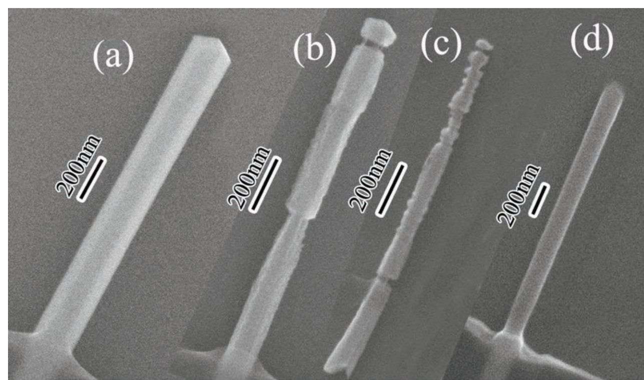

Figure 5. SEM image of GaAs NW a) unetched, b) wet etched for 1 min, c) wet etched for 2 min, and d) milled by FIB.

can be used to quickly check the crystal quality of NWs. However, the nonuniform etch is not suitable for device fabrication. To circumvent this issue, mechanical milling by focus ion beam (FIB) was performed. As can be seen in Figure 5d, after the milling, the NW size is much smaller and still uniform along its length. FIB may cause damage to the crystal lattice of the NWs, which could assist the diffusion of dopants (Zn) into NWs during annealing and benefit the formation of Ohmic contact. Although more studies are needed to confirm this, the good fill factor shown below can suggest the formation of high quality contacts.

On the milled p-NWs, AuZn alloy (Zn% = 5%) was deposited and used as p-contact. After annealing, an n-type contact was subsequently made. The device shown in the inset of **Figure 6**a does not have detectable dark current to the limit of our equipment. When under illumination, it shows a short-circuit photocurrent of $\approx 2 \times 10^{-11}$ A and an open-circuit voltage of ≈0.6 V. The lower photocurrent compared with Reference 41 is because the measurement was performed under much weaker light illumination, and the lower voltage (0.3 V difference) is caused by the lower bandgap of GaAs (1.4 eV) compared with their GaAsP (1.7 eV). The fill factor is 80.5%, the highest reported value for single NW photovoltaics to date. The photoresponse at 0 V bias is shown in Figure 6b, which is very stable during the period of measurement. Step increases or decreases in the illumination produces corresponding steep changes in photocurrent. By lifting one measurement probe to form an open circuit, the measured

© 2018 The Authors. Published by WILEY-VCH Verlag GmbH & Co. KGaA, Weinheim

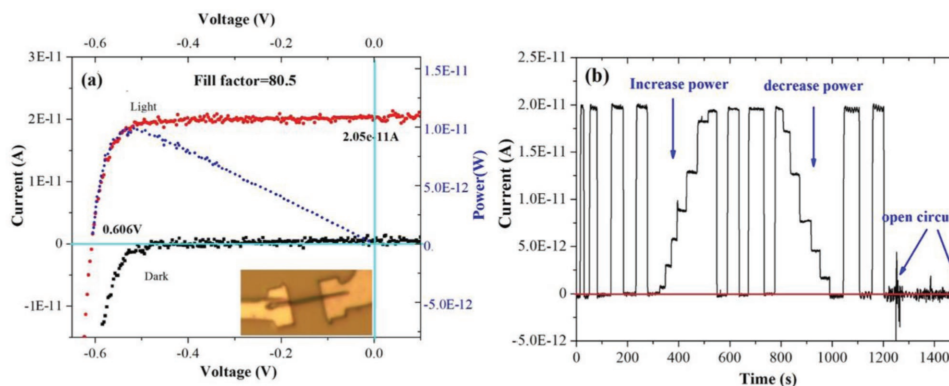

Figure 6. a) Dark/light *I–V* data and *P–V* data of single NW photovoltaic. b) Switching response of the NW device in (a), revealing stability and repeatability of the device as a photodetector.

current is almost the same as the dark current (Figure 6b), which confirms the low current leakage.

In summary, the key factors that can influence the quality of single core–shell p-i-n devices were studied using self-catalyzed GaAs(P) NW photovoltaics, such as p-type doping of core and shell NWs, removal of n- and i-shells, and annealing of the contact. The accumulation of Be inside Ga droplet is a limiting factor that controls the maximum core-NW doping and it becomes more restrictive with higher P content. For shell growth, high Be flux can degrade the morphology, crystal quality, and composition uniformity of NWs with stacking faults. By controlling the Be-doping flux, core–shell NWs with good quality can be grown. On these p-doped NWs, a good Ohmic contact can be achieved even with diameter as small as 50–60 nm, but need annealing under N_2 atmosphere. Therefore, Be doping can be used for constructing core–shell p-i-n junctions in photovoltaics. To make single NW photovoltaics with a radial p-i-n junction, the removal of n- and i-shells to make the p-contact can be performed by mechanical etching, such as milling by FIB. Chemical wet etching is difficult to perform uniformly, because it can be affected by the presence of stacking faults. With these procedures, single NW photovoltaics were fabricated and a world-record high fill factor of 80.5% and stable photoresponse were shown.

Experimental Section

NW Growth: The self-catalyzed GaAs(P) NWs were grown directly on p-type Si(111) substrates by solid-source III–V MBE.[51] If not otherwise noted, the NW growths were using the following parameters. The core GaAsP NWs were grown with a Ga beam equivalent pressure, V/III flux ratio, P/(As+P) flux ratio, and substrate temperature of 8.41×10^{-8} Torr, ≈40, 25%, and ≈640 °C, respectively. The GaAs NWs were grown with a Ga beam equivalent pressure, V/III flux ratio, and substrate temperature of 8.41×10^{-8} Torr, ≈50, and ≈630 °C, respectively. To grow the shell, the Ga droplets were consumed by closing the Ga flux and keeping the group-V fluxes open after the growth of the core. GaAsP shells were then grown with a Ga beam equivalent pressure, V/III flux ratio, P/(As+P) flux ratio, and substrate temperature of 8.41×10^{-8} Torr, 50, 35%, and ≈500 °C, respectively. GaAs shells were grown with a Ga beam equivalent pressure, V/III flux ratio, and substrate temperature of 8.41×10^{-8} Torr, 86, and ≈500 °C, respectively. The substrate temperature was measured by a pyrometer. The GaAs NW photovoltaic was grown with a length of ≈14 µm, and diameter of 340–500 nm. The doping concentration of GaAs p-core, p-shell, and n-shell were 1.6×10^{18} cm^{-3} (Be), 1.6×10^{18} cm^{-3} (Be), and 1×10^{18}–1×10^{19} cm^{-3} (Si), respectively. The thickness ratio of the GaAs p-core, p-shell, and n-shell is 2:3:3. On the p-i-n junction, a layer of ≈30 nm $Al_{0.5}Ga_{0.5}As$ surface passivation layer and a ≈10 nm GaAs protection layer were grown with a Si doping concentration of 1×10^{19} cm^{-3}.

Scanning Electron Microscope (SEM): The NW morphology was measured with a Zeiss XB 1540 FIB/SEM system.

Transmission Electron Microscopy (TEM): Simple scraping of the NWs onto a lacey carbon support was used to prepare TEM specimens. The TEM measurements were performed with a JEOL 2100 and doubly corrected ARM200F microscopes, both operating at 200 kV.

Device Fabrication: The wires were removed from the growth substrate by sonication in isopropanol and drip dried onto strongly p-Si(100) substrates covered with 200 nm thermal SiO_2 and prefabricated Cr/Au pads. The removal of n- and i- shell was performed by Ne FIB milling with a dose of 0.17 nC µm^{-2} using ORION NanoFab. All the contacts were defined using e-beam lithography and then followed by ammonia surface cleaning (NH_3:H_2O = 1:19, 1 min) and subsequent thermal evaporation of contact metals. The p-contact was 500 nm AuZn alloy and the n-contact was 500 nm AuGe alloy. The p-contact/n-contact was annealed for 2 min at 380 /300 °C in a N2 atmosphere.

Device Measurement: The probe station was used for these measurements that equipped with Keithley 4200. The light current was performed under the illumination coupled by Motic MLC-150C box from the GE general electric 35200 model EKE projector light bulb. This bulb had a nominal correlated color temperature of 3250 K and a nominal power of 150 W. The on/off of photoresponse measurements was realized by switching on/off the light manually.

Acknowledgements

Y.Z. designed and fabricated the devices. The authors acknowledge the support of Leverhulme Trust, EPSRC (grant nos. EP/P000916/1 and EP/P000886/1), and EPSRC National Epitaxy Facility.

Conflict of Interest

The authors declare no conflict of interest.

Keywords

contacts, devices, nanowires, photovoltaics, radial p-i-n junctions

Received: September 7, 2018
Revised: November 14, 2018
Published online: December 17, 2018

© 2018 The Authors. Published by WILEY-VCH Verlag GmbH & Co. KGaA, Weinheim

[1] C. M. Lieber, Z. L. Wang, *MRS Bull.* **2007**, *32*, 99.
[2] Y. Zhang, J. Wu, M. Aagesen, H. Liu, *J. Phys. D: Appl. Phys.* **2015**, *48*, 463001.
[3] R. Yan, D. Gargas, P. Yang, *Nat. Photonics* **2009**, *3*, 569.
[4] N. P. Dasgupta, J. Sun, C. Liu, S. Brittman, S. C. Andrews, J. Lim, H. Gao, R. Yan, P. Yang, *Adv. Mater.* **2014**, *26*, 2137.
[5] P. Yang, R. Yan, M. Fardy, *Nano Lett.* **2010**, *10*, 1529.
[6] L. Cao, J. S. White, J. S. Park, J. A. Schuller, B. M. Clemens, M. L. Brongersma, *Nat. Mater.* **2009**, *8*, 643.
[7] S. Mokkapati, C. Jagadish, *Opt. Express* **2016**, *24*, 17345.
[8] P. Krogstrup, H. I. Jørgensen, M. Heiss, O. Demichel, J. V. Holm, M. Aagesen, J. Nygard, A. F. i Morral, *Nat. Photonics* **2013**, *7*, 306.
[9] T. Strudley, T. Zehender, C. Blejean, E. P. Bakkers, O. L. Muskens, *Nat. Photonics* **2013**, *7*, 413.
[10] O. L. Muskens, S. L. Diedenhofen, B. C. Kaas, R. E. Algra, E. P. Bakkers, J. Gómez Rivas, A. Lagendijk, *Nano Lett.* **2009**, *9*, 930.
[11] L. Hu, G. Chen, *Nano Lett.* **2007**, *7*, 3249.
[12] E. Yablonovitch, *J. Opt. Soc. Am.* **1982**, *72*, 899.
[13] P. N. Saeta, V. E. Ferry, D. Pacifici, J. N. Munday, H. A. Atwater, *Opt. Express* **2009**, *17*, 20975.
[14] D. M. Callahan, J. N. Munday, H. A. Atwater, *Nano Lett.* **2012**, *12*, 214.
[15] E. Yablonovitch, G. D. Cody, *IEEE Trans. Electron Devices* **1982**, *29*, 300.
[16] J. D. Christesen, X. Zhang, C. W. Pinion, T. A. Celano, C. J. Flynn, J. F. Cahoon, *Nano Lett.* **2012**, *12*, 6024.
[17] B. M. Kayes, H. A. Atwater, N. S. Lewis, *J. Appl. Phys.* **2005**, *97*, 114302.
[18] P. Lam, S. Hatch, J. Wu, M. Tang, V. G. Dorogan, Y. I. Mazur, G. J. Salamo, I. Ramiro, A. Seeds, H. Liu, *Nano Energy* **2014**, *6*, 159.
[19] S. Hatch, J. Wu, K. Sablon, P. Lam, M. Tang, Q. Jiang, H. Liu, *Opt. Express* **2014**, *22*, A679.
[20] I. Åberg, G. Vescovi, D. Asoli, U. Naseem, J. P. Gilboy, C. Sundvall, A. Dahlgren, K. Svensson, N. Anttu, M. T. Bjork, L. Samuelson, *IEEE J. Photovoltaics* **2016**, *6*, 185.
[21] J. Wallentin, N. Anttu, D. Asoli, M. Huffman, I. Åberg, M. H. Magnusson, G. Siefer, P. FussKailuweit, F. Dimroth, B. Witzigmann, H. Q. Xu, L. Samuelson, K. Deppert, M. T. Borgström, *Science* **2013**, *339*, 1057.
[22] Y. Cui, J. Wang, S. R. Plissard, A. Cavalli, T. T. Vu, R. P. van Veldhoven, L. Gao, M. Trainor, M. A. Verheijen, J. E. M. Haverkort, E. P. A. M. Bakkers, *Nano Lett.* **2013**, *13*, 4113.
[23] M. Yao, N. Huang, S. Cong, C. Y. Chi, M. A. Seyedi, Y. T. Lin, Y. Cao, M. L. Povinelli, P. D. Dapkus, C. Zhou, *Nano Lett.* **2014**, *14*, 3293.
[24] G. Mariani, A. C. Scofield, C. H. Hung, D. L. Huffaker, *Nat. Commun.* **2013**, *4*, 1497.
[25] G. Mariani, P. S. Wong, A. M. Katzenmeyer, F. Léonard, J. Shapiro, D. L. Huffaker, *Nano Lett.* **2011**, *11*, 2490.
[26] M. Yao, S. Cong, S. Arab, N. Huang, M. L. Povinelli, S. B. Cronin, P. D. Dapkus, C. Zhou, *Nano Lett.* **2015**, *15*, 7217.
[27] A. V. Krishnamoorthy, R. Ho, X. Zheng, H. Schwetman, J. Lexau, P. Koka, G. Li, I. Shubin, J. E. Cunningham, *Proc. IEEE* **2009**, *97*, 1337.
[28] C. Colombo, M. Heiβ, M. Grätzel, A. Fontcuberta i Morral, *Appl. Phys. Lett.* **2009**, *94*, 173108.
[29] R. R. LaPierre, A. C. E. Chia, S. J. Gibson, C. M. Haapamaki, J. Boulanger, R. Yee, P. Kuyanov, J. Zhang, N. Tajik, N. Jewell, K. M. Rahman, *Phys. Status Solidi RRL* **2013**, *7*, 815.
[30] G. Otnes, M. T. Borgström, *Nano Today* **2017**, *12*, 31.
[31] E. Barrigon, O. Hultin, D. Lindgren, F. Yadegari, M. H. Magnusson, L. Samuelson, L. I. M. Johansson, M. T. Björk, *Nano Lett.* **2018**, *18*, 1088.
[32] M. Heurlin, P. Wickert, S. Fält, M. T. Borgström, K. Deppert, L. Samuelson, M. H. Magnusson, *Nano Lett.* **2011**, *11*, 2028.
[33] C. Gutsche, A. Lysov, D. Braam, I. Regolin, G. Keller, Z. A. Li, M. Geller, M. Spasova, W. Prost, F. J. Tegude, *Adv. Funct. Mater.* **2012**, *22*, 929.
[34] Y. Dong, B. Tian, T. J. Kempa, C. M. Lieber, *Nano Lett.* **2009**, *9*, 2183.
[35] A. Casadei, P. Krogstrup, M. Heiss, J. A. Röhr, C. Colombo, T. Ruelle, S. Upadhyay, C. B. Sørensen, J. Nygård, A. F. I Morral, *Appl. Phys. Lett.* **2013**, *102*, 013117.
[36] J. Dufouleur, C. Colombo, T. Garma, B. Ketterer, E. Uccelli, M. Nicotra, A. Fontcuberta i Morral, *Nano Lett.* **2010**, *10*, 1734.
[37] Y. Zhang, Z. Sun, A. M. Sanchez, M. Ramsteiner, M. Aagesen, J. Wu, D. Kim, P. Jurczak, S. Huo, L. J. Lauhon, H. Liu, *Nano Lett.* **2018**, *18*, 81.
[38] P. A. Alekseev, M. S. Dunaevskiy, G. E. Cirlin, R. R. Reznik, A. N. Smirnov, D. A. Kirilenko, V. Y. Davydov, V. L. Berkovits, *Nanotechnology* **2018**, *29*, 314003.
[39] H. Ali, Y. Zhang, J. Tang, K. Peng, S. Sun, Y. Sun, F. Song, A. Falak, S. Wu, C. Qian, M. Wang, Z. Zuo, K. J. Jin, A. M. Sanchez, H. Liu, X. Xu, *Small* **2018**, *14*, 1704429.
[40] O. Demichel, M. Heiss, J. Bleuse, H. Mariette, A. Fontcuberta i Morral, *Appl. Phys. Lett.* **2010**, *97*, 201907.
[41] J. V. Holm, H. I. Jørgensen, P. Krogstrup, J. Nygård, H. Liu, M. Aagesen, *Nat. Commun.* **2013**, *4*, 1498.
[42] R. R. LaPierre, *J. Appl. Phys.* **2011**, *110*, 014310.
[43] J. Wu, A. Ramsay, A. Sanchez, Y. Zhang, D. Kim, F. Brossard, X. Hu, M. Benamara, M. E. Ware, Y. I. Mazur, G. J. Salamo, M. Aagesen, Z. Wang, H. Liu, *Nano Lett.* **2016**, *16*, 504.
[44] V. A. Nebol'Sin, A. A. Shchetinin, *Inorg. Mater.* **2003**, *39*, 899.
[45] Y. Zhang, A. M. Sanchez, J. Wu, M. Aagesen, J. V. Holm, R. Beanland, T. Ward, H. Liu, *Nano Lett.* **2015**, *15*, 3128.
[46] M. Paladugu, J. Zou, Y. N. Guo, X. Zhang, H. J. Joyce, Q. Gao, H. H. Tan, C. C. Jagadish, Y. Kim, *Angew. Chem., Int. Ed.* **2009**, *48*, 780.
[47] B. Paulus, P. Fulde, H. Stoll, *Phys. Rev. B* **1996**, *54*, 2556.
[48] A. Gaymann, M. Maier, K. Köhler, *J. Appl. Phys.* **1999**, *86*, 4312.
[49] M. Gutieŕrez, D. Araujo, P. Jurczak, J. Wu, H. Liu, *Appl. Phys. Lett.* **2017**, *110*, 092103.
[50] J. C. Garcia, E. Rosencher, P. Collot, N. Laurent, J. L. Guyaux, B. Vinter, J. Nagle, *Appl. Phys. Lett.* **1997**, *71*, 3752.
[51] Y. Zhang, A. M. Sanchez, Y. Sun, J. Wu, M. Aagesen, S. Huo, H. Liu, *Nano Lett.* **2016**, *16*, 1237.

© 2018 The Authors. Published by WILEY-VCH Verlag GmbH & Co. KGaA, Weinheim